Biosensors and Bioelectronics 128 (2019) 23–31

Contents lists available at ScienceDirect

Biosensors and Bioelectronics

journal homepage: www.elsevier.com/locate/bios

Reduced graphene oxide doping with nanometer-sized ferrocene moieties – New active material for glucose redox sensors

Edyta Matysiak-Brynda[a,1,*], Jakub P. Sęk[a,1], Artur Kasprzak[b], Agata Królikowska[a], Mikolaj Donten[c], Michał Patrzalek[c], Magdalena Poplawska[b], Anna M. Nowicka[a]

[a] Faculty of Chemistry, University of Warsaw, Pasteura 1 Str., PL-02-093 Warsaw, Poland
[b] Faculty of Chemistry, Warsaw University of Technology, Noakowskiego 3 Str., PL-00-664 Warsaw, Poland
[c] Faculty of Chemistry, Biological and Chemical Research Centre, University of Warsaw, Żwirki i Wigury 101 Str., 02-089 Warsaw, Poland

ARTICLE INFO

Keywords:
rGO doped with ferrocene
Raman spectroscopy
Microscopic analysis
Glucose oxidase
Glucose detection

ABSTRACT

Herein, we present that the reduced graphene oxide (rGO) doped with nanometer-sized ferrocene moieties is a new, excellent active material for redox sensors. Two distinct approaches were utilized for the modification of rGO. The first method was based on the covalent decoration of rGO *via* the addition of azomethine ylide generated from the ferrocenecarboxaldehyde oxime. The second approach utilized the adsorption of 1,1′-ferrocenedicarboxylic acid on the graphene sheet *via* the π-π stacking. The morphology of the synthesized graphene materials was studied by application of microscopic techniques, whereas the Raman data allowed the characteristics of the tested materials in terms of their structural properties. The tested graphene materials doped with ferrocene moieties were used as a bioactive platform for glucose oxidase (GOx) immobilization. The enzyme was immobilized onto the rGO materials in two ways: (i) using a crosslinking agent – glutaraldehyde (GA) and (ii) by formation of the amide bonds between carboxylic groups of rGO-Fc$(COOH)_2$ and amine groups from enzyme. Ferrocene moieties present at the graphene surface play the role of mediator in the electron transfer between the redox center of GOx and the electrode surface. The functionality of the constructed biosensors has been tested on real samples. The results of the recovery rates showed a satisfying degree of accuracy toward determination of glucose concentration. Examination of the potential interfering species has demonstrated favorable sensitivity and selectivity of the designed biosensor for the detection of glucose.

1. Introduction

Diabetes is an extremely serious chronic disease that can cause many complications, such as heart attack, stroke, kidney failure or nerve damage (Hu et al., 2013; Cao et al., 2013; Liu et al., 2018). Therefore, the determination of blood glucose is important in fighting diabetes, especially at an early stage. Due to the fact that other components present in a blood sample may interfere in terms of the determination of glucose in a real sample, there is an urgent need to develop and to apply rapid, very sensitive and selective methods for determining this blood sugar (Monosik et al., 2012; Liu et al., 2018). Biosensors belong to the class of very efficient analytical tools that allow the monitoring of the discreet changes of the amount of glucose in the real samples, mainly in the blood. Despite an intensive research in the recent years, the construction of the desired tool was not achieved. Therefore, rapid, selective, inexpensive and easy to perform protocols for determination of glucose are still needed. The electrochemical biosensors are the most promising devices, especially in the terms of their high sensitivity, simplicity of measurement and low cost of analysis (Stradiotto et al., 2003; Parlak et al., 2017). The most popular electrochemical biosensors for determining the amount of glucose in the blood utilize a synergistic mechanism of operation, based on an enzymatic reaction coupled with an amperometric detection (Guadarrama-Fernández et al., 2018). These types of biosensors are usually based on the glucose oxidase (GOx) and are widely used due to their high specificity, relatively low cost and good stability (Chen et al., 2015). In case of using this enzyme, the direct electron transfer between GOx and electrode surface is very difficult, because the electroactive site of GOx is deeply embedded in the enzyme shell (Riklin et al., 1995; Kang et al., 2009; Mu et al., 2007). Therefore, to facilitate the exchange of electrons between the active center of the enzyme and the electrode surface, the mediators are commonly used (Zang et al., 2007; Liu et al.,

* Corresponding author.
E-mail address: ematysiak@chem.uw.edu.pl (E. Matysiak-Brynda).
[1] These authors contributed equally.

https://doi.org/10.1016/j.bios.2018.12.037
Received 29 October 2018; Received in revised form 12 December 2018; Accepted 14 December 2018
Available online 27 December 2018
0956-5663/

2009). One of the most popular mediators used in the construction of amperometric biosensors are the ferrocene derivatives (Senel, 2011).

The search for new materials and methods to increase the sensitivity, selectivity and stability of the biosensors is still a major challenge for researchers. Graphene–family materials have been attracting great interest with the regard to their outstanding electronic and optical properties (Gholampour et al., 2017; Kasprzak and Poplawska, 2018). Graphene is a promising material for electrochemical applications, because it has high surface area and high electrical conductivity (Stankovich et al., 2006). Nevertheless, graphene monolayers are very expensive in production and difficult to handle. However, they can be successfully changed to reduce flake graphene (4–10 graphene monolayers), which had similar properties as graphene monolayer (Tang et al., 2009).

In pursuit of construction of a highly selective and sensitive electrochemical biosensor for glucose determination in serum, the reduced graphene oxide (rGO) doped with unsubstituted ferrocene (rGO-Fc) and ferrocene with two carboxylic groups (rGO-Fc$(COOH)_2$) were used as a matrix for glucose oxidase immobilization. The detection of glucose was based on tracking oxidation current of ferrocene moieties; it resulted in the increase of its amperometric signal in the presence of glucose in the solution. The proposed biosensors have been characterized using various techniques.

2. Experimental section

The details about used chemicals, procedure of the synthesis of rGO doping with nanometer-sized ferrocene moieties and applied techniques are given in SI, Section 1.

3. Results and discussion

3.1. Characterization of rGO, rGO-Fc and rGO-Fc$(COOH)_2$ materials

3.1.1. IR analysis

Two distinct approaches were utilized for the modification of rGO. The first method was based on the covalent decoration of rGO *via* the addition of azomethine ylide generated from the ferrocenecarboxaldehyde oxime. The second approach utilized the adsorption of 1,1′-ferrocenedicarboxylic acid on the graphene sheet *via* the π-π stacking. In the spectrum of rGO-Fc (Fig. 1S in SI), the peak located at 1550 cm^{-1} is ascribed to the N-C vibrations coming from the *N*-methylpyrrolidine ring on the graphene sheet. It confirms that Fc has been indeed covalently anchored to the rGO. In the spectrum of rGO-Fc$(COOH)_2$ the absorption band located at 1695 cm^{-1} is ascribed to the $-C^{=}O$ vibrations coming from the $-COOH$ groups of Fc$(COOH)_2$. It confirms that the Fc$(COOH)_2$ has been adsorbed on the surface of rGO *via* the π-π stacking

3.1.2. Electron microscopy examinations

To monitor the changes in the rGO structure upon its doping with ferrocene moieties, the electron microscopic examination were done. Fig. 1A-C shows a comparison of TEM images taken for all three materials. They prove appearance of wrinkles on a larger scale (hundreds of nanometers) presented in upper row, and smaller (several nm) dimples found in modified materials, detected also using SEM (Fig. 2S in SI). It is worth to stress that appearance of those nanometric structures is the best pronounced for rGO doped with Fc$(COOH)_2$. The evidence of merging ferrocene to modified rGO was found in EDS mapping, with the aid of TEM observations performed in scanning technique (STEM). The obtained results are displayed in Fig. 3S in SI. More details about electron microscopic analysis are given in SI, Section 2. Concluding, three findings can be drawn from electron microscopy observations: (i) the native rGO material has multiplanar structure, consisting of well-defined graphene layers; (ii) modification of the rGO with Fc and Fc$(COOH)_2$ leads to stiffening of rGO flakes and appearance of nanometric dimples on its surface; (iii) Fc and Fc$(COOH)_2$ attached to rGO in the modification procedure concentrates with in the rGO as uniformly spread dimples.

3.1.3. Raman spectroscopy analysis

Raman spectroscopy provided further insight into the structural features and electronic properties of rGO and their changes upon modification with Fc and Fc$(COOH)_2$. Two types of the samples were examined: solid powders of rGO; rGO-Fc and rGO-Fc$(COOH)_2$, compared with neat Fc and (Fc-$(COOH)_2$ as control samples (Fig. 5S and 6S in SI) and rGO, rGO-Fc and rGO-Fc$(COOH)_2$ deposited as thin films on silicon support, to eliminate the spectral interference of the GC substrate (Fig. 7S in SI). A successful functionalization of rGO with ferrocene derivatives was confirmed indirectly for the powders, with Raman signature of the decomposition product (iron carbide). (Fig. 5S and 6S in SI). A detailed assignment and discussion of the Raman spectra is given in Section 2.1., SI. The most informative Raman spectral parameters are listed in Table 1 for the solid samples (part A) and films on Si (part B). In case of the powder samples, a more disrupted and disordered structure was deduced for rGO-Fc$(COOH)_2$ due to the downshift and broadening of the D peak (see the legend of Table 1 and SI for the labels of rGO Raman peaks) comparing to rGO and rGO-Fc. The increase in the I_D/I_G ratio (Table 1A) for rGO upon doping with ferrocene derivative (clearly more pronounced for the rGO-Fc$(COOH)_2$ solid sample) indicated the increased number of the defects within graphene sheets (Ashwin Karthick et al., 2018). For the thin films, covalent linking with Fc had larger effect on the original structure of rGO than π-π stacking involving rGO and Fc$(COOH)_2$, as demonstrated by the changed I_D/I_G ratio and shift of D and G bands (Table 1B). Meticulous analysis of the second order peaks (Section XX, SI) showed that in this case the increased I_D/I_G ratio is a signature of more ordered state of rGO-Fc$(COOH)_2$, comparing to rGO and rGO-Fc. A lowered C/O content was derived from the Raman data (King et al., 2016) for rGO-Fc $(COOH)_2$ with respect to rGO and rGo-Fc, which suggests the best conductivity of this material among studied samples (Morimoto et al., 2016).

3.2. Glucose biosensor

The procedure of preparation of electrochemical glucose biosensors with rGO doped with ferrocene moieties is described in SI (Section 2) and illustrated in Fig. 2A. In the case of the construction of the electrochemical bioactive platforms it is essential to permanently anchor the enzyme and other electrochemical moieties onto the surface of the electrode. In the case of GC/rGO-Fc$(COOH)_2$ layer, the glucose oxidase was introduced onto the electrode surface through the amide bond, which was formed between the amine groups of the enzyme and the carboxylic groups of ferrocene moieties at rGO sheets. In turn, to attach the glucose oxidase to GC/rGO or GC/rGO-Fc layer the electrode was immersed in the mixture containing GOx (C_{GOx} = 5 mg mL^{-1}) and 10% GA (cross-linking agent) for 24 h at the 4 °C. Glutaraldehyde is a well-known bifunctional crosslinker for the covalent immobilization studies, due to its ability to react mainly with highly nucleophilic amine groups from glucose oxidase and partially with the weakly nucleophilic hydroxyl groups present at the surface of reduced graphene oxide (Buhus et al., 2009; Bahar, 2016). In our case, the reaction between Fc moieties and GA clearly does not take place, because of the lack of the reactive nucleophilic partner for GA in Fc's structure. As a consequence, the obtained crosslinked materials have a complex structure. They are considered to be interpenetrated–interconnected networks. It is also known that the ratio of the enzyme content to the content of the crosslinking agent plays a key role in maintaining of the biological activity of the enzyme (Chui and Wan, 1997). Low concentration of crosslinking agent in comparison to the enzyme concentration, is insufficient to form a three-dimensional network, while the high concentration of GA may result in a distortion of the enzyme structure *i.e.,*

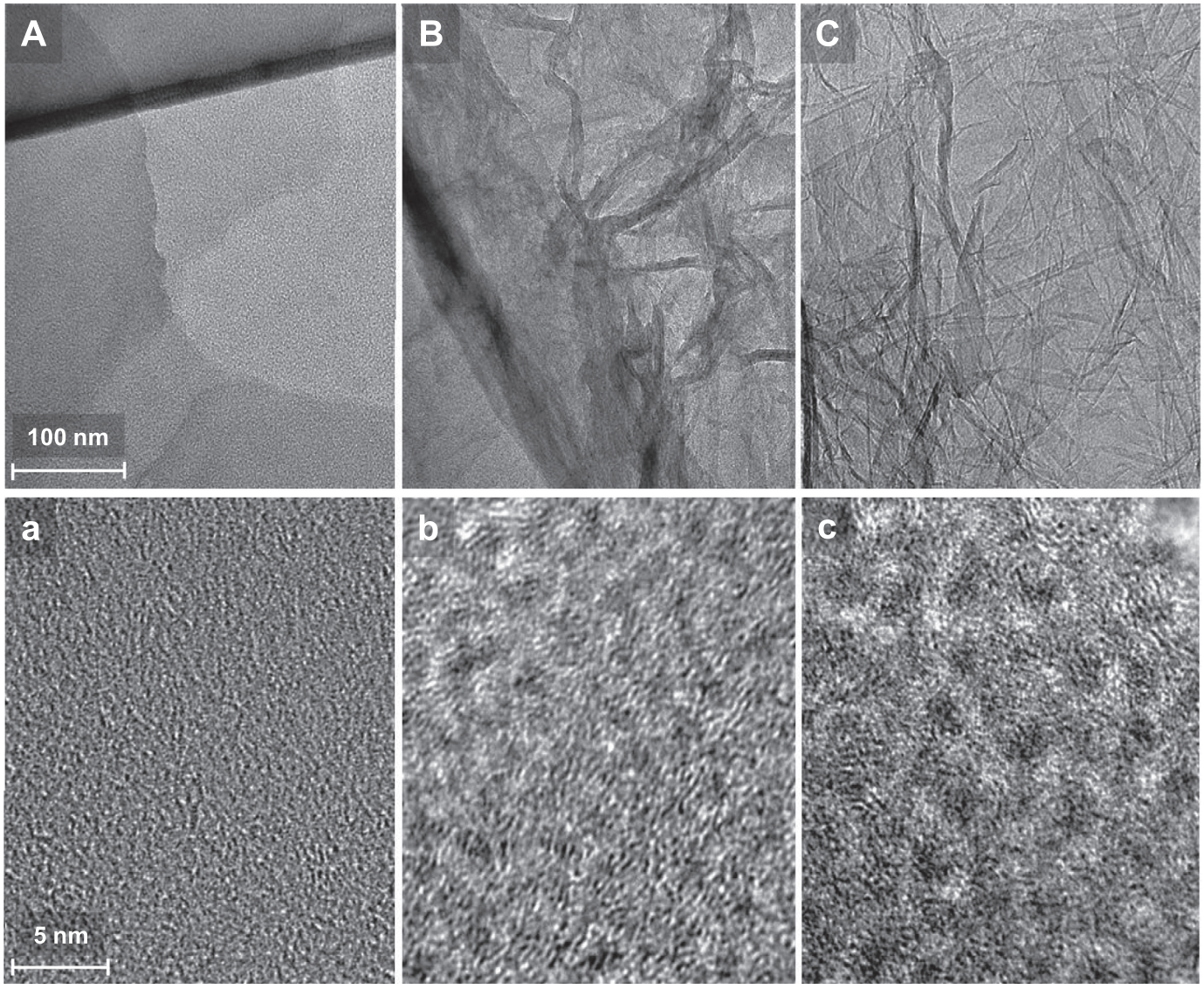

Fig. 1. TEM images of (A) unmodified rGO, (B) rGO-Fc and (C) rGO-Fc(COOH)$_2$. Lower row (a-c) presents HRTEM images of magnified areas selected from materials shown in upper row.

the active site conformation (Broun, 1976). The concentration ratio applied in our studied of GA to GOx guaranteed the formation the very tight three-dimensional network, labelled as "GOx-GA", that contributes to keeping the high activity of the enzyme (Migneault et al., 2004; Jensen et al., 2012).

To get the information about enzyme packing in the layer formed by covalent anchoring of GOx on the rGO-Fc(COOH)$_2$ layer, the QCM-D measurements were performed. For this purpose the gold crystal was first modified by rGO-Fc(COOH)$_2$ layer, employing a physical adsorption. Then, the carboxylic groups were activated by standard reagents, mixture of 10 mM NHS/40 mM EDC and such modified piezoelectrode was placed in the QCM-D chamber. Fig. 3A shows typical QCM-D spectra of the frequency (Δf) and the dissipation factor (ΔD) changes during covalent binding of GOx to rGO-Fc(COOH)$_2$ layer for various overtones. After stabilization of the frequency and the dissipation factor in 0.02 M PBS buffer, the immobilization process of enzyme was initiated by adding the GOx to the buffer (0.50 mg mL^{-1}). The rapid and significant drop in Δf confirmed the covalent bonding of GOx to the carboxylic groups, functionalizing the ferrocene units present at the rGO surface. After *ca.* 2 h the frequency shift reached a stable value, which meant that the tightly packed film of enzyme was formed at the electrode surface. Moreover, the frequency changes for different overtones did not differ significantly, so it can be assumed that formed enzyme layer is homogenous, and quite well-packed.

GOx from *Aspergillus niger* is a dimeric globular protein; the single monomer has an elliptical shape with dimensions 6.4 × 4.7 × 3.8 nm (x, y, z) (Fogel et al., 2007). Considering the elliptical shape of this enzyme, we can distinguish three GOx orientations on the surface, which are presented in the inset of Fig. 3A. Using the formula for the ellipse area ($A_{\text{theoret. GOx}} = \pi \times a \times b$, see the inset in Fig. 3A) the theoretical surface area occupied by one molecule of GOx for each orientation was calculated, which is equaled 14.0 (y, z), 19.1 (x, z) and 23.6 (x, y) for A, B and C orientation, respectively. On the bases of the dimension of GOx dimer and its molecular weight of ~160 kDa (M_W = 159,970.9 g mol^{-1}), the theoretical frequency shifts corresponding to the formation of a close packed GOx monolayer in each orientation (here we use an RSA model (Adamczyk and Weroński, 1996) of protein adsorption) can be determined and are equal to: −58.5, −43.0 and −34.8 for the orientations A, B and C, respectively. It should be stressed that the RSA model can be applied to the monodispersed spherical or ellipsoidal objects as a 2D deposition model where the objects are hard spheres and do not move. The estimated theoretical Δf value (−34.8 Hz) is in good agreement with the experimental data, which confirmed the GOx molecules are covalently bound to the rGO-Fc

Table 1
Raman bands parameters and I_D/I_G ratios for: (A) the solid powder samples and (B) the samples of thin films on Si substrate.

A: Raman bands parameters and I_D/I_G ratios for the solid powder samples

Sample type (solid powder)	Raman spectrum parameter (633 nm)			
	D band position [cm^{-1}]	FWHM[a] D band [cm^{-1}]	G band position [cm^{-1}]	I_D/I_G ratio (integrated area)
rGO	1335	116	1592	1.35
rGO-Fc	1335	112	1592	1.67
rGO-Fc $(COOH)_2$	1328	143	1592	3.42

B: Raman bands parameters and I_D/I_G ratios for the samples of thin films on Si substrate

Sample type (thin film on Si)	Raman spectrum parameter								
	D band position [cm^{-1}]	G band position [cm^{-1}]	I_D/I_G ratio[b]	A_D/A_G ratio[c]	D band position [cm^{-1}]	G_{app} band position [cm^{-1}]	I_D/I_{Gapp} ratio	2D' [cm^{-1}]	D'_{inf}-G_{app} [cm^{-1}]
	633 nm				532 nm				
rGO	1335	1590	1.24	0.87	1347	1590	0.63	3200	10
rGO-Fc	1335	1590	1.24	0.79	1347	1588	0.66	3199	11
rGO-Fc$(COOH)_2$	1335	1590	1.35	0.94	1342	1585	0.88	3199	14

a - Full width at half maximum, b - Integral intensity, c - Amplitude ratio.
Legend for the Raman labels of rGO bands:
D- disorder peak, G – graphite/graphene peak, D′ disorder peak for highly defected graphene, 2D′ – overtone of D′mode, G_{app} – apparent position of the G peak, due to superposition of the G and D′ modes, D'_{inf} - the inferred position of D′ mode, extracted by halving the energy of 2D' peak.

$(COOH)_2$ layer, adapting the orientation C.

More information about the morphology of the GOx layer can be obtained from the plot of ΔD *versus* Δf presented in Fig. 3B. From the dependency of $\Delta D = f(\Delta f)$ two distinct regions, shifted with respect to each other are visible. This behavior may be interpreted as a fact of formation of the adlayer or the monolayer with different distance from the electrode surface. Taking into account the slopes of these ranges, which are very similar, it suggests that a monolayer was formed. The shift of the linear ranges at Fig. 3B can be ascribed to different arrangement of Fc moieties within the graphene layer (the two possible boundary orientations are shown in the inset of the Fig. 3B).

3.2.1. Analytical performance

The analytical characteristics based on the chronoamperometric measurements was performed for two platforms for GOx immobilization: rGO-Fc and rGO-Fc$(COOH)_2$. The potential equal to 0.35 V for GC/rGO-Fc and GC/rGO-Fc$(COOH)_2$ biosensor was applied, based on the CV curves (Fig. 4A), in the chronoamperometric studies. The rGO unmodified by Fc was used as a control material to confirm that the electron exchange between enzyme and electrode surface indeed take place through Fc moieties. The mechanism of action of the developed biosensors is presented in Fig. 2B.

The typical calibration curves of the GC/rGO-Fc/GA-GOx biosensor were recorded in 0.02 M PBS buffer at pH 7.4 and 1000-fold diluted rat serum. The results for the glucose concentration ranging from 1 to 300 μM are shown in Fig. 4B. The sensor shows linear response in two ranges from 2 to 10 μM and from 20 to 100 μM. In addition, these two regimes in the calibration curves are characterized by a different slope, which can be caused by a different catalytic activity of the immobilized glucose oxidase at the rGO-Fc layer in the solution with low and high concentration of glucose. Probably, the presence of two ranges of the linearity is associated with the different number of active sites in the enzyme structure with respect to the amount of glucose in the solution, and as a consequence the different efficiency of the glucose oxidation by the enzyme. The slope of the first calibration curve is high for the lower concentration of glucose in the solution, probably due to a high number of active sites in glucose oxidase. In the case of higher concentration of glucose, the sensitivity of the second calibration curve declines, due to decreasing number of the active sites in the enzyme structure (Arvand and Hemmati, 2017). The detection limit (LOD) was determined from the low concentration linearity range of the calibration curve according to the equation:

$$LOD = \frac{3\sigma}{a} \quad (1)$$

where σ is the standard deviation of the response and a is the slope of the calibration curve. The determined LOD equaled to 0.02 μM in deoxygenated PBS buffer and 0.06 μM in the presence of oxygen. In the case of measurements performed in rat serum the limits of detection (LOD) were 0.03 and 0.04 μM in deoxygenated and oxygen saturated solutions, respectively. For the higher values of glucose concentration (> 100 μM) no significant changes in the intensity of the recorded current signal were observed. It means that glucose oxidase has its maximum catalytic activity at low glucose concentration up to *ca.* 100 μM. Moreover, the presence of oxygen affects slightly the values of current, what is probably related to the fact that in a presence of oxygen there is high competition between the mediator and the oxygen in the solution which has an influence on the activity of glucose oxidase (Toghill and Compton, 2010).

The biosensor with the glucose oxidase covalently anchored to electrode modified with GC/rGO-Fc$(COOH)_2$/GOx was characterized by 20 times lower values of ferrocene oxidation currents in comparison to the biosensor with enzyme immobilization with glutaraldehyde, see Fig. 4C. The lowering of observed current values is probably related to the quantity of the covalently anchored enzyme. The presence of oxygen in the solution had slight effect on the oxidation current of ferrocene, mostly in the case of measurements performed in the rat serum. These currents were slightly higher than currents obtained for the deoxygenated solution. The linear dependence of Fc oxidation signal as a function of the glucose concentration was observed for the two ranges of glucose concentrations from 1 to 10 μM and from 20 to 100 μM, as in the case of GC/rGO-Fc$(COOH)_2$/GOx biosensors. The limits of detection were *ca.* 0.04 and 0.02 μM in deoxygenated and oxygen saturated PBS buffer, respectively. In the rat serum the detection limits were equal to 0.02 and 0.01 μM in the presence of Ar and O_2, respectively.

The control experiment with pure rGO material was performed to ensure that the electron exchange between the glucose oxidase and the electrode surface has mediated character. The observed current changes at the 0.35 V were insignificant in comparison to the rGO materials doped with ferrocene moieties, see Fig. 4D. The very small current values proved that efficiency of the electron exchange between the

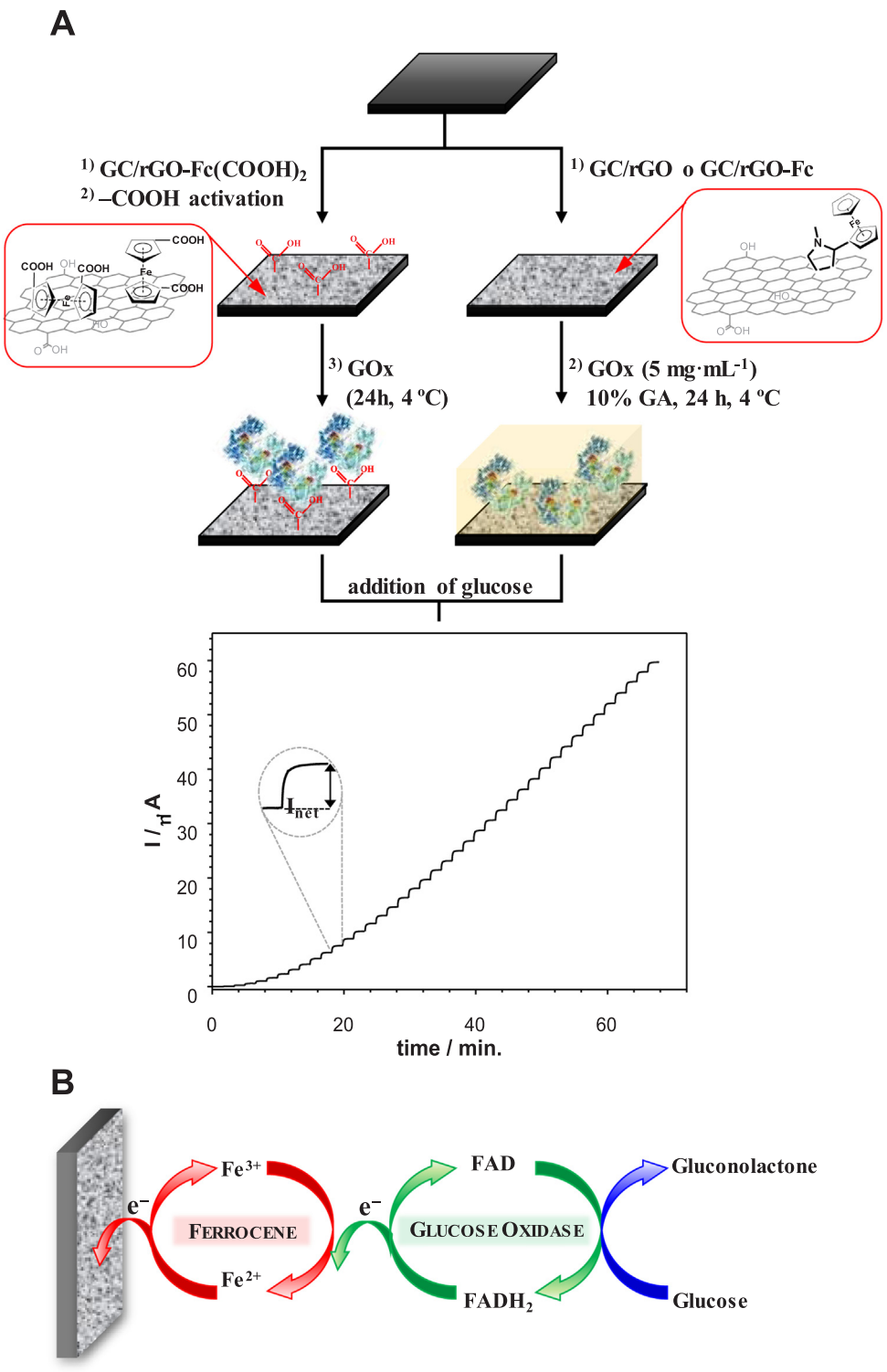

Fig. 2. (A) Scheme of biosensors construction for glucose detection and (B) mechanism of electron exchange between GOx and electrode surface through Fc moieties in the presence of glucose in the solution.

enzyme redox center and the electrode surface in the absence of the mediator is very poor. It confirms our thesis of the crucial role of ferrocene residues for the proper action of the developed biosensors.

The calibration equations for GC/rGO-Fc/GA-GOx and GC/rGO-Fc $(COOH)_2$/GOx biosensors in the PBS buffer and rat serum are given in Table 1S in SI. The low values of RSD (< 8%) reflect the good precision of the proposed biosensors. For all tested glucose biosensors when the glucose concentration exceeds 100 µM, the observed current approached a plateau with the increasing glucose concentration, which shows a typical Michaelis-Menten kinetic mechanism (Çakiroğlu and Özacar, 2017). The Michaelis-Menten constant (K_m), which determines the affinity of the substrate to the enzyme, was calculated to evaluate the biological activity of GOx immobilized on the electrode surface, using the Lineweaver-Burk equation given below: (Lineweaver and Burk, 1934)

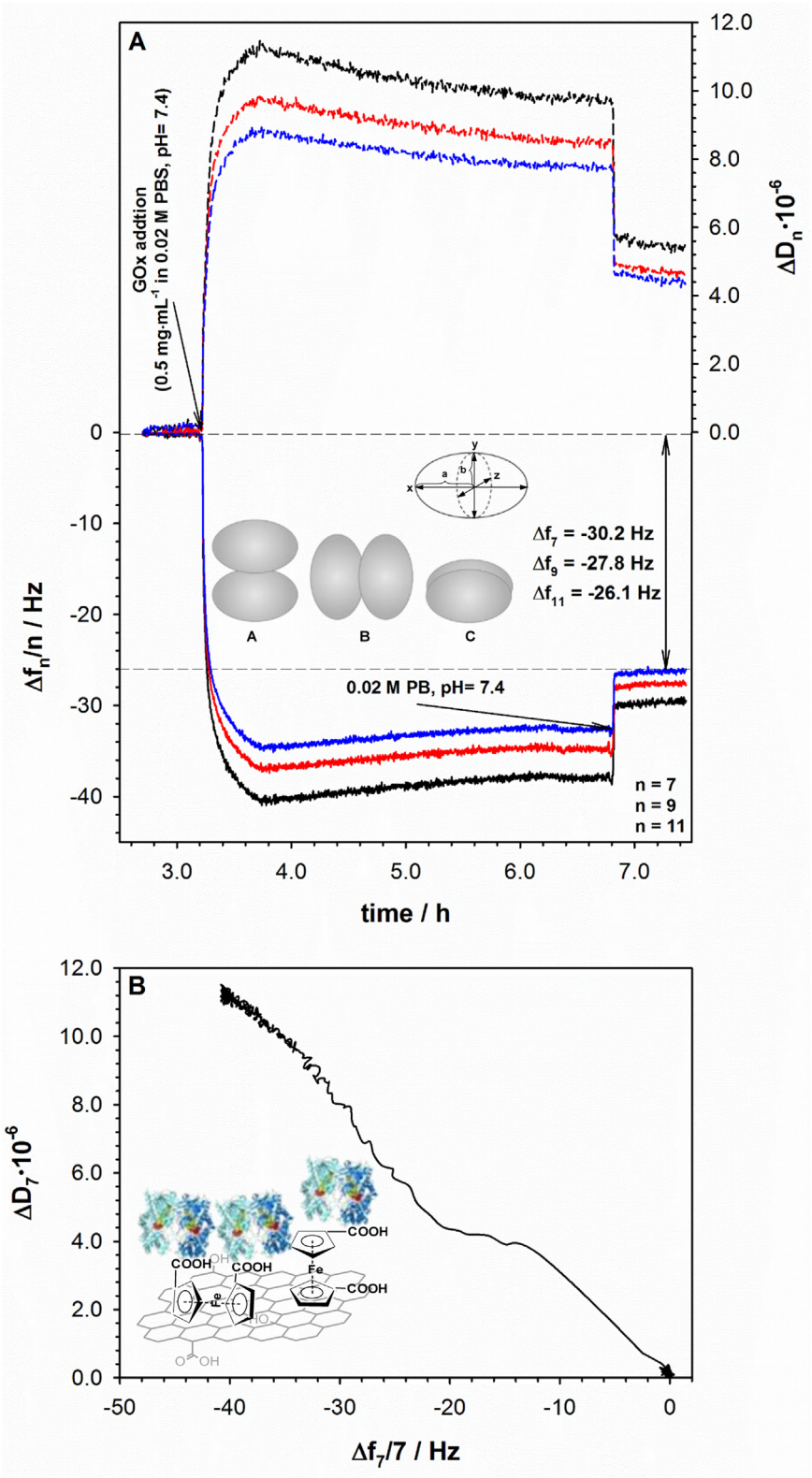

Fig. 3. (A) Typical QCM-D spectra of the shifts in frequency (Δ*f*) and dissipation factor (Δ*D*) during formation of GOx layer on modified gold electrode surface (Au/rGO-Fc(COOH)$_2$). Inset: three major possible conformations of GOx at substrate surface. (B) Δ*D versus* Δ*f* plots of GOx covalent attachment to modified electrode surface (Au/rGO-Fc(COOH)$_2$). Experimental conditions: C_{GOx} = 0.50 mg mL^{-1}; 0.02 M PBS buffer at pH 7.4; wash out buffer: 0.02 M phosphate buffer (PB).

$$\frac{1}{I} = \frac{K_m}{I_{max}} \cdot \frac{1}{C} + \frac{1}{I_{max}} \quad (2)$$

where I is the steady-state response current after the addition of glucose, C is the glucose concentration and I_{max} is the saturation current. The determined K_m values were not greater than 4.5 μM, see Table 1S in SI. The obtained values are much smaller than K_m constants described in the literature for other GOx based glucose biosensors (0.22, 8.2, 4.6 mM) (Liu et al., 2005; Zhao et al., 2006; Mao et al., 2018). Such

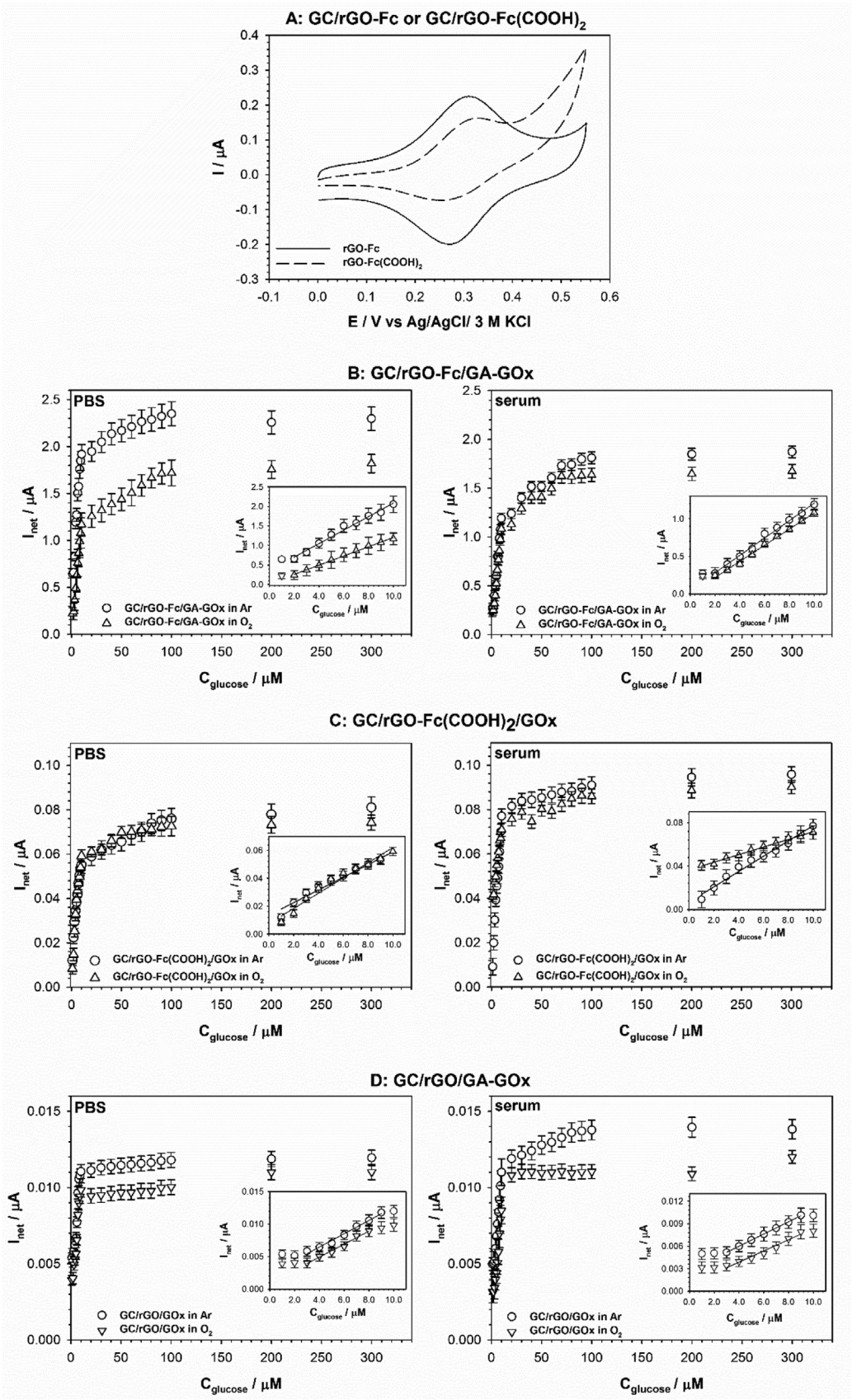

Fig. 4. (A) Representative background subtracted CV voltammograms of rGO-Fc and rGO-Fc(COOH)$_2$ immobilized onto glassy carbon electrode surface. Experimental conditions: 0.02 M PBS buffer, pH 7.4; $C_{\text{rGO-Fc}} = 0.125\ \text{mg mL}^{-1}$, $C_{\text{rGO-Fc(COOH)}_2} = 0.125\ \text{mg mL}^{-1}$, $\nu = 25\ \text{mV s}^{-1}$. Calibration plots of the changes in the net oxidation current of ferrocene at 0.35 V for (B) GC/rGO-Fc/GA-GOx, (C) GC/rGO-Fc(COOH)$_2$/GOx and (D) GC/rGO/GA-GOx biosensors in the addition of increasing concentrations of glucose in the presence and absence of oxygen in 0.02 M PBS buffer at pH 7.4 and 1000-fold diluted rat serum. Insets: the calibration curves for the lower linearity range.

Table 2
Electrochemical methods for glucose detection.

Analytically active layer	Method	Signal transducer	Analytical range [μM]	LOD [μM]	Ref.
Mediated electron exchange					
GC/Fc-bPEI-AuNPs/GOx	ChA	Fc	500–10,000	40	(Mao et al., 2018)
SPCE/PAA-rGO/VS-PANI/$LuPc_2$/MFH-GOx	ChA	$LuPc_2$	2000–12,000	25	(Dilusha Cooray et al., 2016)
GC/poly(Py/Py-COOH/Py-Fc)/GOx	ChA	Fc	1000–4000	6.9	(Al-Sagur et al., 2017)
GC/Th/Th-COOH/Th-Fc/GOx	ChA	Fc	500–3000	2.5	(Şenel, 2011)
ITO/poly(Py-PyFc)/GOx	ChA	Fc	2500–16,800	170	(Abasıyanık and Şenel, 2010)
GC/rGO-Fc/GA-GOx	ChA	Fc	2–10	0.02	This work
GC/rGO-Fc$(COOH)_2$/GOx	ChA	Fc	1–10	0.04	This work
Direct electron exchange					
GC/MWCNTs-Py/GOx	ChA	GOx	3–700	–	(Palomera et al., 2011)
GC/rGO-PAMAM-Ag/GOx	ChA	GOx	32–1890	4.5	(Chen et al., 2015)
GC/chitosan/ TiO_2-TCS/GOx	ChA	GOx	5–1320	2.0	(Luo et al., 2012)
GC/p-NiO/n-$Bi_4Ti_3O_{12}$/GOx	ChA	GOx	20–3550	1.3	(Yang et al., 2014)
GC/AuNPs/GNT/GOx	ChA	GOx	10–2000	4.1	(Devasenathipathy et al., 2015)

GC: glassy carbon electrode; Fc: ferrocene; bPEI: branched polyethylenimine; AuNPs: gold nanoparticles; GOx: glucose oxidase; ChA: chronoamperometry; SPCE: screen printed carbon electrode; PAA: polyacrylic acid; rGO: reduced graphene oxide; VS-PANI: vinyl substituted polyaniline; $LuPc_2$: lutetium phthalocyanine; MFH: multifunctional hydrogel; Py: pyrrole; Py-COOH: 3-(1H-pyrrol-1-yl)propanoic acid; Py-Fc: *N*-(3-(1H-pyrrol-1-yl)ethyl)ferrocenecarboxlate; Th: thiophene, Th-COOH: thiophene-3-acetic acid; Th-Fc: dicyclopentadienyl iron-1,4-dienylmethyl-2-(thiophen-3-yl)acetate; ITO: indium tin oxide; MWCNTs: multi-wall carbon nanotubes; PAMAM: poly(amidoamine); Ag: silver; TCS: tetragonal columnar-shaped with TiO_2 nanorods; p-NiO: NiO p-type semiconductor; n-$Bi_4Ti_3O_{12}$: $Bi_4Ti_3O_{12}$ n-type semiconductor; GNT: graphene nanotubes.

small values of the K_m constants indicate that the here proposed biosensors are marked by the stronger affinity towards the glucose substrate and in consequence the immobilized GOx exhibits a higher enzymatic activity. The limits of detection of the proposed biosensors of glucose determination remained at the lower or similar level to the other electrochemical approaches described in the literature (Table 2).

3.2.2. Selectivity and functionality of the glucose biosensors

In order to study the selectivity of the GC/rGO-Fc/GA-GOx and GC/rGO-Fc$(COOH)_2$/GOx biosensors the amperometric response of the sensor upon the addition of typical interferences such as fructose, ascorbic acid and uric acid to the glucose solution was verified. Due to the fact that the concentrations of the selected interferents in the blood serum differ from each other, the examination was done for equimolar solution of both glucose and the interferent (5 μM) and for excess of interfernts at normal level: fructose (10 μM), ascorbic acid (100 μM) and uric acid (200 μM) in blood serum.

The amperometric measurements were done in the 0.02 M PBS buffer at the potential of 0.35 V. The influence of the investigated interferents on the recorded current signal ($I_{net\ +\ interferent}/I_{net}$) is shown in Fig. 8S in SI, Section 2.2. The obtained data show that the presence of fructose, ascorbic acid and uric acid even at the normal level in blood (excess towards glucose) only slightly influenced the current signal of ferrocene.

The functionality of the proposed biosensors was checked on two real samples: rat serum and orange juice. Due to the rich matrix of the real samples in the first step, to minimize the process of blocking of the electrode surface by other species, the rat serum and orange juice were diluted by 0.02 M PBS buffer 1000-fold and 100-fold, respectively. The concentration of glucose in deoxygenated rat serum determined by proposed biosensors were found to be 4.2 ± 0.8 and 4.6 ± 0.5 μM for GC/rGO-Fc/GA-GOx and GC/rGO-Fc$(COOH)_2$/GOx, respectively. The concentration of glucose in deoxygenated orange juice were: 3.2 ± 0.6 for GC/rGO-Fc/GA-GOx and 4.1 ± 0.8 μM for GC/rGO-Fc$(COOH)_2$/GOx. The real concentration of glucose was *ca.* 4.7 mM in rat serum and *ca.* 0.38 mM in orange juice, so the obtained results show clearly that the proposed procedure is selective enough and can be successfully used for the determination of glucose in real samples.

The information about the stability of the proposed sensors, intraday and interday precisions and the recovery of glucose in the natural samples (serum and juice) is given in SI, Section 2.3.

4. Conclusions

These studies provides fundamental insight into the influence of the way of modification of the graphene-family material by the redox probe on its structural and electronic properties, toward its applicability for the biosensor construction. First of all, the modification of rGO by ferrocene moieties leads to the rigidification of graphene sheet and the appearance of nanometric-scale dimples on the surface of the modified samples. Secondly, the electronic properties of rGO are also changed upon doping. These changes are directly associated with the applied synthetic approach. The Raman spectra elucidated that the rGO-Fc$(COOH)_2$ material exhibits better conductivity than rGO-Fc platform.

The most prominent achievement of this work is that here proposed bioactive platforms, based on reduced graphene oxide doping with nanometer-sized ferrocene, exhibit higher affinity of the glucose oxidase to glucose comparing to the previously reported sensors. Besides, it was demonstrated that the presence of oxygen and other substances in the sample, usually coexisting with glucose in real samples, has a legible effect on the analytical signals. Therefore, the determination of glucose with our biosensors is possible at very low level (0.03 μM) in the real samples, together without extensive sample preparation. We believe that this simple approach, combining excellent sensitivity and specificity, is potentially a promising alternative to the amperometric detection, employed currently in glucose biosensors.

CRediT authorship contribution statement

Edyta Matysiak-Brynda: Methodology, Investigation, Writing - original draft, Writing - review & editing. **Jakub P. Sęk:** Investigation, Validation, Visualization. **Artur Kasprzak:** Investigation, Visualization, Writing - original draft. **Agata Królikowska:** Investigation, Visualization, Writing - original draft. **Mikolaj Donten:** Investigation, Visualization, Writing - original draft. **Michał Patrzalek:** Investigation. **Magdalena Poplawska:** Writing - review & editing, Validation. **Anna M. Nowicka:** Conceptualization, Writing - original draft, Writing - review & editing, Supervision, Resources, Funding acquisition.

Acknowledgements

Support for this work by a National Science Centre of Poland, Grant no. 2014/15/D/ST4/02989 is gratefully acknowledged. The SEM/TEM

images were obtained using the equipment purchased within CePT Project no. POIG.02.02.00-14-024/08-00. The QCM-D measurements were performed using the equipment purchased within National Science Centre of Poland Project no. 2015/19/B/ST5/03530. Artur Kasprzak acknowledges Foundation for Polish Science (FNP) for the START scholarship, and National Science Centre of Poland for the Etiuda Scholarship (no. 2018/28/T/ST5/00018).

Declaration of interest statement

None.

Appendix A. Supporting information

Supplementary data associated with this article can be found in the online version at https://doi.org/10.1016/j.bios.2018.12.037.

References

Abasıyanık, M.F., Şenel, M., 2010. J. Electroanal. Chem. 639, 21–26.
Adamczyk, Z., Weroński, P., 1996. J. Chem. Phys. 105, 5562–5573.
Al-Sagur, H., Komathi, S., Khan, M.A., Gurek, A.G., Hassan, A., 2017. Biosens. Bioelectron. 92, 638–645.
Arvand, M., Hemmati, S., 2017. Sens. Actuators B 238, 346–356.
Ashwin Karthick, N., Thangappan, R., Arivanandhan, M., Gnanamani, A., Jayavel, R., 2018. J. Inorg. Organomet. Polym. Mater. 3, 1021–1028.
Bahar, T., 2016. Asia-Pac. J. Chem. Eng. 11, 981–988.
Broun, G.B., 1976. Chemically aggregated enzymes. In: Mosbach, K. (Ed.), Methods in Enzymology. Academic Press, New York, pp. 263–280.
Buhus, G., Popa, M., Desbrieres, J., 2009. J. Bioact. Compat. Pol. 24, 525–545.
Çakiroğlu, B., Özacar, M., 2017. Electroanalytical 29, 2719–2726.
Cao, X., Wang, N., Jia, S., Shao, Y., 2013. Anal. Chem. 85, 5040–5046.
Chen, H.-C., Tu, Y.-M., Hou, C.-C., Lin, Y.-C., Chen, C.–H., Yang, K.-H., 2015. Anal. Chim. Acta 867, 83–91.
Chui, W.K., Wan, L.S., 1997. J. Microencapsul. 14, 51–61.
Devasenathipathy, R., Mani, V., Chen, S.M., Huang, S.T., Huang, T.T., Lin, C.M., Hwa, K.Y., Chen, T.Y., Chen, B.J., 2015. Enzym. Microb. Technol. 78, 40–45.
Dilusha Cooray, M.C., Sandanayake, S., Li, F., Langford, S.J., Bond, A.M., Zhang, J., 2016. Electroanalytical 28, 2728–2736.
Fogel, R., Mashazi, P., Nyokong, T., Limson, J., 2007. Biosens. Bioelectron. 23, 95–101.
Gholampour, A., Kiamahalleh, M.V., Tran, D.N.H., Ozbakkaloglu, T., Losic, D., 2017. ACS Appl. Mater. Interfaces 9, 43275–43286.
Guadarrama-Fernández, L., Novell, M., Blondeau, P., Andrade, F.J.A., 2018. Food Chem. 265, 64–69.
Hu, Y.M., Jiang, X.M., Zhang, L.Y., Fran, J., Wu, W.T., 2013. Biosens. Bioelectron. 48, 94–99.
Jensen, U.B., Vagin, M., Koroleva, O., Sutherland, D.S., Besenbacher, F., Ferapontova, E.E., 2012. J. Electroanal. Chem. 667, 11–18.
Kang, X.H., Wang, J., Wu, H., Aksay, I., Liu, J., Lin, Y.H., 2009. Biosens. Bioelectron. 25, 901–905.
Kasprzak, A., Poplawska, M., 2018. Chem. Commun. 54, 8547–8562.
King, A.A.K., Davies, B.R., Noorbehesht, N., Newman, P., Church, T.L., Harris, A.T., Razal, J.M., Minett, A.I., 2016. Sci. Rep. 6, 19491.
Lineweaver, H., Burk, D., 1934. J. Am. Chem. Soc. 56, 658–666.
Liu, J., Guo, C., Li, C.M., Li, Y., Li, Y., Chi, Q., Huang, X., 2009. Electrochem. Commun. 11, 202–205.
Liu, W., Ding, F., Wang, Y., Mao, L., Liang, R., Zou, P., Wang, X., Zhao, Q., Rao, H., 2018. Sens. Actuators B 265, 310–317.
Liu, Y., Wang, M., Zhao, F., Xu, Z., Dong, S., 2005. Biosens. Bioelectron. 21, 984–988.
Luo, Z., Yuwen, L., Han, Y., Tian, J., Zhu, X., Weng, L., Wang, L., 2012. Biosens. Bioelectron. 36, 179–185.
Mao, W., Cai, B., Ye, Z., Huang, J., 2018. Sens. Actuators B 261, 385–391.
Migneault, I., Dartiguenave, C., Bertrand, M.J., Waldron, K.C., 2004. BioTechniques 37, 790–802.
Monosik, R., Stredansky, M., Tkac, J., Sturdik, E., 2012. Food Anal. Method 5, 40–53.
Morimoto, N., Kubo, T., Nishina, Y., 2016. Sci. Rep. 6, 21715/1–21715/8.
Mu, C., Zhao, Q., Xu, D., Zhuang, Q., Shao, Y., 2007. J. Phys. Chem. B 111, 1491–1495.
Palomera, N., Vera, J.L., Meléndez, E., Ramirez-Vick, J.E., Tomar, M.S., Arya, S.K., Singh, S.P., 2011. J. Electroanal. Chem. 658, 33–37.
Parlak, O., Incel, A., Uzun, L., Turner, A.P.F., Tiwari, A., 2017. Biosens. Bioelectron. 89, 545–550.
Riklin, A., Katz, E., Wiliner, I., Stocker, A., Bückmann, A.F., 1995. Nature 376, 672–675.
Senel, M., 2011. Synth. Met. 161, 1861–1868.
Stankovich, S., Dikin, D.A., Dommett, G.H.B., Kohlhaas, K.M., Zimney, E.J., Stach, E.A., Piner, R.D., Nguyen, S.T., Ruoff, R.S., 2006. Nature 442, 282–286.
Stradiotto, N.R., Yamanaka, H., Zanoni, M.V.B., 2003. J. Braz. Chem. Soc. 14, 159–173.
Tang, L., Wang, Y., Li, Y., Feng, H., Lu, J., Li, J., 2009. Adv. Funct. Mater. 19, 2782–2789.
Toghill, K.E., Compton, R.G., 2010. Int. J. Electrochem. Sci. 5, 1246–1301.
Yang, Z., Tang, Y., Li, J., Zhang, Y., Hu, X., 2014. Biosens. Bioelectron. 54, 528–533.
Zang, J., Li, C.M., Cui, X.Q., Wang, J.X., Sun, X.W., Dong, H., Sun, C.Q., 2007. Electroanalytical 19, 1008–1014.
Zhao, S., Zhang, K., Bai, Y., Yang, W., Sun, C., 2006. Bioelectrochemistry 69, 158–163.